

Structure and properties of (TiVCrZrY)N coatings prepared by energetic bombardment sputtering with different nitrogen flow ratios

Du-Cheng Tsai · Zue-Chin Chang · Bing-Hau Kuo ·
Ming-Hua Shiao · Shou-Yi Chang · Fuh-Sheng Shieu

Received: 2 June 2013 / Accepted: 28 August 2013 / Published online: 13 September 2013
© Springer-Verlag Berlin Heidelberg 2013

Abstract (TiVCrZrY)N coatings were deposited onto Si substrate by the radio-frequency (RF) magnetron sputtering of a TiVCrZrY alloy target in an N₂/Ar atmosphere. The crystal, microstructural, mechanical, and electrical properties at different N₂-to-total (N₂+Ar) flow-rate ratio (R_N) values were investigated. The coating produced in pure Ar had an equiaxed structure with a hexagonal-close-packed phase. With increased R_N , the crystallinity and grain size markedly decreased. The microstructure of (TiVCrZrY)N coatings transformed from V-shaped columnar with a rough-domed surface into fine fibrous with a smooth surface. The amorphous transition layer above the substrate was also significantly thickened. The hardness of (TiVCrZrY)N decreased from 20.9 GPa to 18.9 GPa, and the electrical resistivity increased from 398.2 $\mu\Omega\cdot\text{cm}$ to 21870 $\mu\Omega\cdot\text{cm}$.

1 Introduction

A protective surface coating intends to provide a layer of protection from anything that can damage the function or integrity of an item. The application of a surface coating is common in a number of different fields, including cutting and forming tools, machinery components, aerospace, and automotive parts. Protective surface coatings also help maintain the functionality of materials, i.e., their high hardness, wear resistance, thermal stability, oxidation resistance, and chemical stability, under severe conditions and over prolonged lifetimes. Common deposition techniques for fabricating a surface coating with desired properties include cathode arc deposition, ion plating, and magnetron sputtering. To enhance the performance of particular tools, dies, and molds for several applications, the protective coating technology is continually being developed.

Since the 1980s, binary transition metal nitrides such as TiN, CrN, and ZrN have been widely used in industries [1–3]. However, the demand for higher performance has required the addition of different elements to the existing nitride to modify its properties for specific applications. The best known example is the incorporation of Al atoms into a TiN lattice. This procedure has been successfully commercialized particularly for high-speed machining applications because of the resultant improvement in oxidation resistance and mechanical properties [4–6]. The former is due to the formation of a protective Al-rich oxide layer on the coating surface. The latter is attributed to the solid-solution strengthening effect. The addition of other elements such as Cr, Zr, or Ta to form a ternary system has been previously shown to generate superior performance [7–9]. Accordingly, alloying nitride coatings with appropriate elements is an effective method of modifying the coating properties. Recently, Yeh et al. developed sputtered multielement

D.-C. Tsai · B.-H. Kuo · S.-Y. Chang · F.-S. Shieu (✉)
Department of Materials Science and Engineering, National
Chung Hsing University, Taichung 40227, Taiwan
e-mail: fsshieu@dragon.nchu.edu.tw
Fax: +886-4-22857017

F.-S. Shieu
Center of Nanoscience & Nanotechnology, National Chung Hsing
University, Taichung 40227, Taiwan

Z.-C. Chang
Department of Mechanical Engineering, National Chin-Yi
University of Technology, Taichung 41170, Taiwan

M.-H. Shiao
Instrument Technology Research Center, National Applied
Research Laboratories, Hsinchu 300, Taiwan

nitride coatings with more than five elements using a multielement target. Multielement nitride coatings have high mixing entropy and thus tend to form simple solid-solution phase, which enables an easy analysis, control, and development of these coatings. Previous studies have revealed that (AlCrMnMoNiZr)N, (AlCrNbSiTiV)N, (AlCrMoTaTiZr)N, (AlMoNbSiTaTiVZr)N, and (TiVCrZrHf)N possess beneficial features and properties [10–14]. They are of great interest as hard coatings because of their good mechanical properties induced by strong solid-solution strengthening, grain-boundary hardening, and even nanocomposite structures.

Indeed, suitable materials for high-entropy nitrides have been screened. TiN, CrN, and ZrN have been developed and used as mechanically and chemically protective layers for industrial applications because of their satisfactory mechanical properties. Adding one more metal element to form Ti, Cr, and Zr-based ternary nitride coatings reportedly result in improved properties compared with the binary compound [7–9]. For example, the incorporation of V into the cubic nitride structure can enhance mechanical and tribological properties [15]. However, in the case of Y, important information is very limited. The addition of the large-sized Y to multielement nitride is expected to exert a remarkable effect on resultant structure and properties.

Recent studies show that the (TiVCrZrY)N coating without a substrate bias and/or heating achieves a pronounced hardness of 17.5 GPa when the N₂-to-total (N₂+Ar) flow-rate ratio (R_N) is 100 % [16]. However, further improvement in mechanical properties and detailed investigations on the role of Y addition are still needed. In this study, deposition time was controlled to produce a coating with the same coating thickness to the ignore thickness effect. R_N strongly influences the structure and properties. Accordingly, nitride coatings under various R_N values were prepared to determine the effect of R_N during film formation on the structural, mechanical, and electrical properties of the resultant (TiVCrZrY)N coatings.

2 Experimental

(TiVCrZrY)N coatings were deposited onto p-Si (100) wafers using a radio-frequency (RF) magnetron sputtering system with equimolar TiVCrZrY targets 50 mm in diameter. Before deposition, the Si substrates were cleaned and then rinsed with ethanol and distilled water in an ultrasonic bath. The (TiVCrZrY)N coatings were deposited at room temperature in an Ar+N₂ atmosphere under an RF power of 150 W and a working pressure of 6×10^{-3} torr. The bias of the substrate was fixed at -100 V. During deposition, the total gas flow-rate ratio was fixed at 30 sccm, and the R_N was varied from 0 % to 50 %. The deposition time was increased with increased R_N to control the coating thickness

at around 500 nm. The targets were presputtered with Ar to remove their surface oxide layers before deposition.

The chemical compositions of the coatings were determined by field-emission electron probe microanalyses (FE-EPMA, JOEL JXA-8800M). At least three tests were performed for each sample. As a rough approximation, the relative error is about ± 1 at.%. The error bars cannot be observed because the size of the error bars is smaller than the size of the symbols. The crystal structures were analyzed with a glancing-incidence (1°) X-ray diffractometer (XRD, BRUKER D8 Discover) using Cu K α radiation at a scanning speed of $1^\circ/\text{min}$. Furthermore, the average grain sizes of the coatings were calculated based on the full-width at half-maximum using the Scherrer formula [17]. Morphology studies and thickness measurements were carried out using FE scanning electron microscopy (SEM, JEOL JSM-6700F). Meanwhile, the deposition rate was obtained by dividing the thickness by the deposition time. Microstructural examinations were conducted using an analytical transmission electron microscope (TEM, FEI E.O. Tecnai F20). The surface roughness (root mean square) values of the coatings were derived with an atomic force microscope (AFM, Seiko SPA400). The microhardness and elastic modulus of the coatings were measured using a TriboLab nanoindenter (Hysitron). At least five tests were performed for each sample. The electrical resistivity of the coatings was measured using a four-point probe system.

3 Results and discussion

3.1 Crystal structure

Figure 1 presents EPMA of the constituent element in (TiVCrZrY)N coatings deposited at various R_N values. The oxygen concentration in these coatings was less than 4 at.%. The alloy coating was in a near-equimolar ratio and close to the designed values. With the introduction of nitrogen, less variation existed in the representation of target elements in the resulting coatings. The concentration of nitrogen and target elements is almost not affected by R_N and has nearly stoichiometric ratio of (TiVCrZrY)₅₀N₅₀. This information helps eliminate the contribution of structure and properties due to composition difference in the coatings at various R_N , which is in agreement with the report by Huang and Yeh [11]. Figure 2 reveals the variation of the deposition rate with R_N . The deposition rate decreases from 14.1 to 6.3 nm/min when R_N is increased from 0 to 50 %. This is probably attributed to a lower sputtering yield resulting from the nitrogen absorption or even nitridation of the metal target and/or the reduced sputtering efficiency of reactive gas ions [18].

Figure 3 presents the XRD pattern of (TiVCrZrY)N coatings deposited at various R_N . For TiVCrZrY alloy coating,

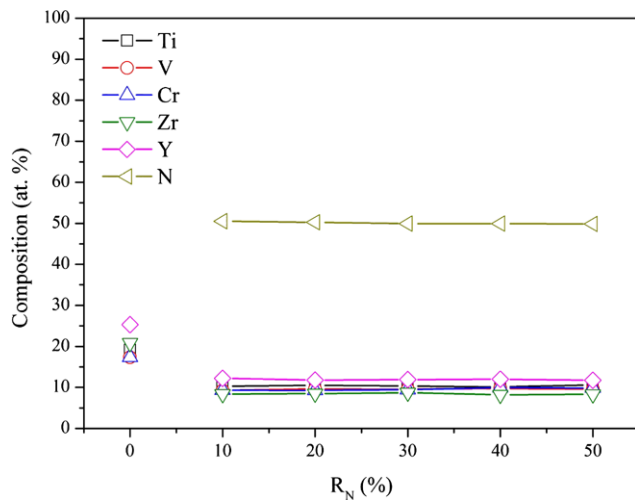


Fig. 1 Chemical compositions in (TiVCrZrY)N coating deposited at various R_N

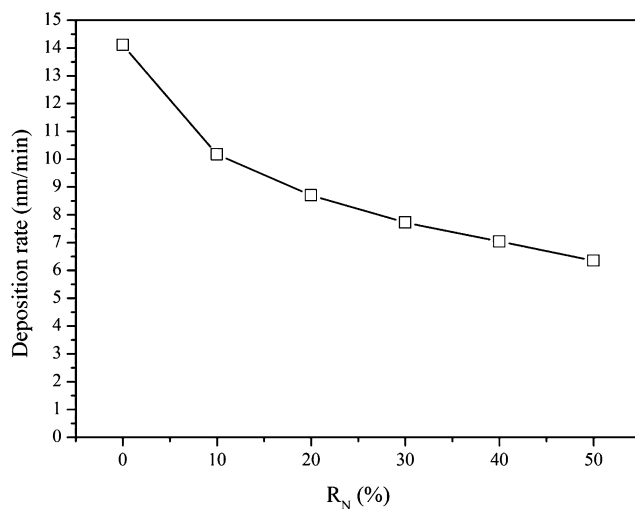


Fig. 2 Deposition rate of (TiVCrZrY)N coating deposited at various R_N

two broad peaks representing the hexagonal close-packed (hcp) crystal structure was found [19]. This finding can be attributed to the incorporation of large amounts of Ti, Zr, and Y into the hcp crystal structure. For TiVCrZrY nitride coatings, a mixed structure of NaCl-type face-centered cubic (fcc) phase and near-amorphous phase were observed. This fcc solid solution formed because TiN, VN, CrN, ZrN, and YN all have an fcc phase. Previous reports describe similar observations on ternary nitrides and other multielement nitrides, such as (TiCr)N, (CrV)N, (TiZr)N, (ZrY)N, (TiVCr)N, and (TiVCrZrHf)N [9, 14, 15, 20, 21]. Table 1 lists the lattice constant of the TiVCrZrY nitride coating theoretically calculated according to the Vegard rule, along with the EPMA-determined composition. Table 2 presents experimentally measured lattice constant derived from the lattice spacing in the [200] orientation of XRD pattern of the

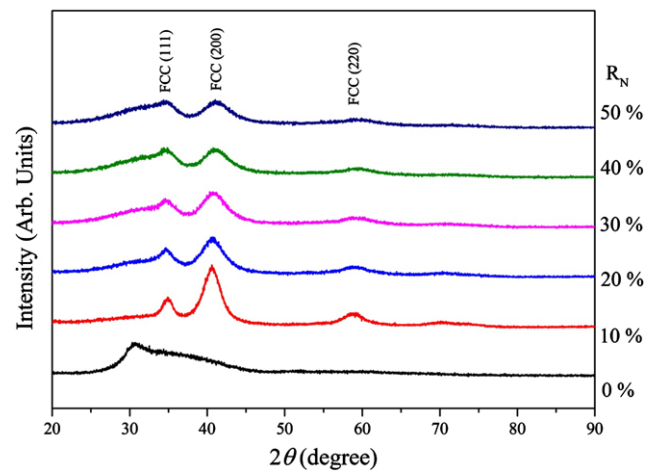


Fig. 3 X-ray diffraction patterns of the (TiVCrZrY)N coatings deposited at various R_N

TiVCrZrY nitride crystals. The calculated lattice constants were consistent with the measured values. This finding indicated the formation of a solid solution from all constituted nitrides; the atoms of five metallic elements randomly occupied the metal-atom positions [20].

In terms of crystallinity, Table 2 shows that the (TiVCrZrY)N coatings had a (200) preferred orientation. Some researchers on the NaCl-type structure posit that preferred orientation occurs because of the anisotropy between the surface energy and strain energy. If the surface energy is dominant during coating growth, the (200) plane with the lowest surface energy preferentially develops [22]. Thus, the preferential grain growth was surface-energy dominant in our case. As R_N increased, the number of crystalline structures and grain size decreased (increased amorphous content). As aforementioned, the reduction in the deposition rate of the target at higher R_N induced more energetic bombardment on the growing coatings. Associated with the application of a substrate bias of -100 V, this resputtering effect was expected to occur and gradually increase with increased R_N ; consequently, grain growth was inhibited [11, 20, 23]. Another observation from the XRD patterns was that the diffraction peak shifted to higher angles with increased R_N , which implied a decrease in the lattice parameter. Composition variation should be negligible since coatings at various R_N have similar compositions. From TEM observations (Figs. 5, 6 and 7), densification of coating is considered to be minor factor since the voids along the boundaries occupy only a very small volume fraction. Therefore, the lattice decline may be explained by the increase of intrinsic compressive stress caused by enhance energetic bombardment.

Previous reports indicate that for high-entropy nitride coatings such as (AlCrNbSiTiV)N, (AlCrMoTaTiZr)N, (AlMoNbSiTaTiVZr)N, and (TiVCrZrHf)N, their minimal grain sizes are 8.7, 14.3, 9.5, and 6.2 nm, respectively [11–14, 24]. Compared with the (TiVCrZrY)N coating in our

Table 1 Theoretically lattice constant (*a*) of individual nitrides and (TiVCrZrY)N coating deposited at $R_N = 30\%$

	Element					
	TiN	VN	CrN	ZrN	YN	(TiVCrZrY)N
	Crystal structure					
	FCC	FCC	FCC	FCC	FCC	FCC
<i>a</i> (Å)	4.2417	4.1392	4.1400	4.5740	4.8944	4.4132

Table 2 Relative intensities of diffraction peaks, average grain sizes, and lattice constant of (TiVCrZrY)N coatings

R_N (%)	Relative intensity				Average grain size (nm)	Lattice constant (Å)
	(100)	(002)	(110)	(111)		
0	224.8	178.1			1.5	$a = 3.2803$ $b = 4.7298$
	(111)	(200)	(220)	Amorphous peak		
10	132.0	682.0	130.4	198.5	3.5	4.4384
20	180.9	534.1	129.1	266.8	2.7	4.4288
30	148.2	491.8	113.3	363.9	2.5	4.4086
40	131.5	398.4	111.3	437.1	2.3	4.3795
50	108.7	366.7	97.1	457.8	2.2	4.3716

study, these reported coatings have a relatively large grain size and better crystallinity. The incorporation of Y atoms with the large atomic radius of 1.802 Å may be the main reason. High-entropy nitride coatings are known to favor the formation of an fcc solid solution structure. However, a high mixing entropy is not the only factor that controls solid-solution formation in multielement materials. The atomic size difference should also be considered as the critical parameter that determines the formation of a solid solution or amorphous phase. Zhang et al. [25] defined the atomic size difference by the following equation:

$$\text{Atomic size difference} = 100 \sqrt{\sum_{i=1}^n c_i (1 - r_i/\bar{r})^2},$$

where c_i and r_i are the atomic percentage and atomic radius of the i th element. The numerical factor 100 was used to amplify the data for clarity. Based on the above equation, the atomic size differences among AlCrNbSiTiV, AlCrMoTaTiZr, AlMoNbSiTaTiVZr, TiVCrZrHf, and TiVCrZrY were estimated to be 8.35, 7.48, 8.66, 9.70, and 13.43, respectively. Evidently, severe lattice distortion caused by a large atomic size difference led to an amorphous tendency. The results found were similar to those of Braic et al. [26]. However, further research and development in the multielement nitride coatings would still be required.

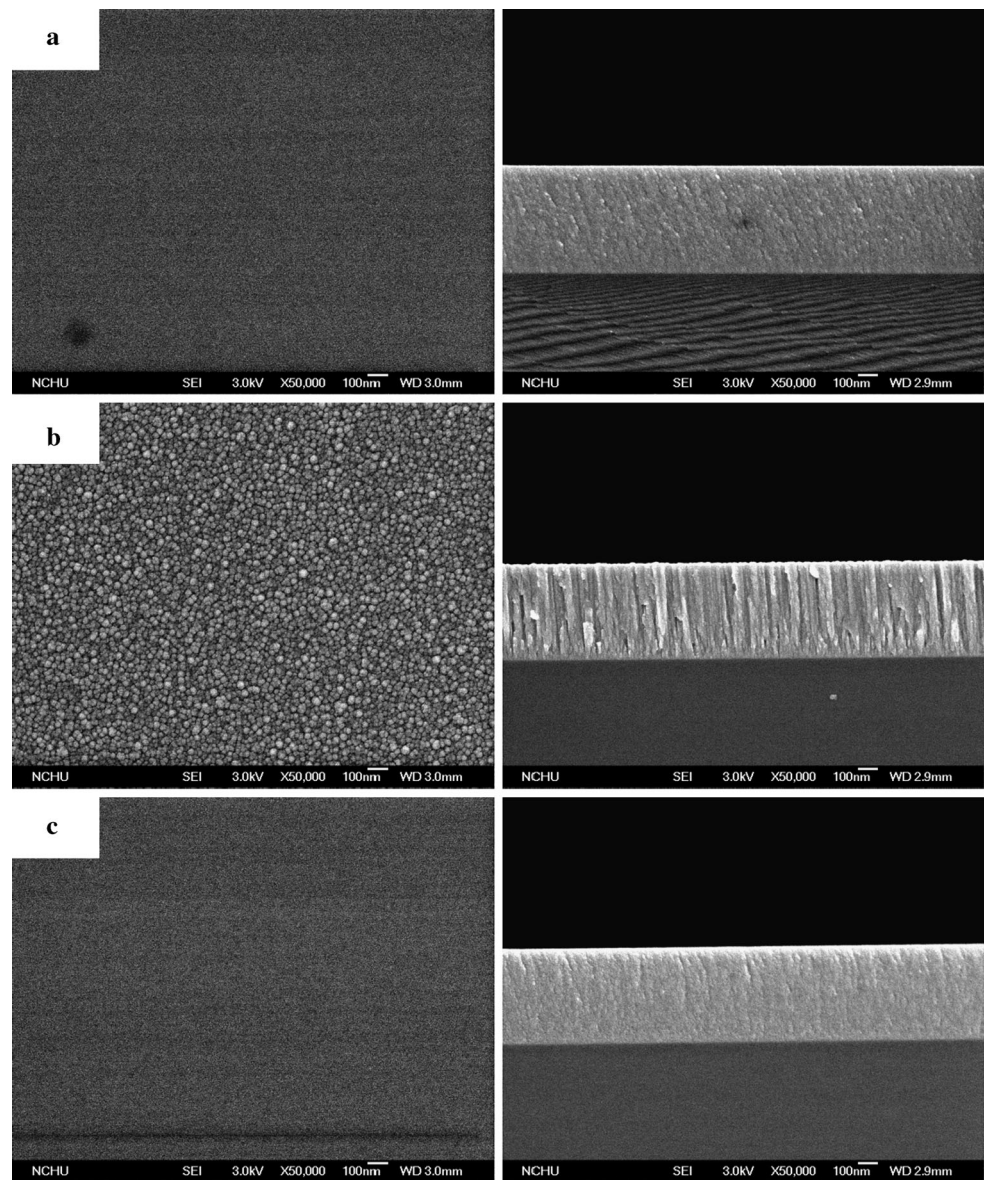
3.2 Microstructure

Figure 4 shows the plan-view and cross-sectional SEM micrographs of (TiVCrZrY)N coatings deposited at various R_N values. For the TiVCrZrY alloy coating deposited at

$R_N = 0\%$, a granular structure with a very small surface roughness of 0.3 nm was observed. When $R_N = 10\%$, the nitride coating displayed a columnar structure with a domed surface feature and a high surface roughness of 2.6 nm. With increased R_N to 50%, the surface morphology became smooth, and the original columnar structure was inhibited. The surface roughness of the coating was as small as only ~ 0.3 . To understand further the structural evolution of (TiVCrZrY)N coatings, TEM was used to observe the microstructure and texture through the thickness direction.

Figures 5, 6 and 7 illustrate the TEM images with selected area diffraction (SAD) patterns of (TiVCrZrY)N coating deposited at $R_N = 0\%$, 10%, and 50%, respectively. The TiVCrZrY alloy coatings had a dense, glass-like structure (Fig. 5a). However, further TEM and SAD observations revealed two distinct layers in the coatings (Figs. 5b–d). The lower part had an amorphous structure approximately 380-nm thick, whereas the upper part had an equiaxed structure (crystallites size < 5 nm) with an hcp phase (100) preferred orientation. The top part of the coating structure was confirmed to contain an hcp (100)-axis structure perpendicular to the substrate misaligned at $\sim 60^\circ$ (Fig. 5d). The interplanar distance among the crystallites was approximately 0.283 nm (Fig. 5f). The thick amorphous layer and extremely small crystallites can be attributed to the large differences among the atomic size and crystal structure of the elements. For the nitride formed at $R_N = 10\%$, a V-shaped columnar structure with dense grain boundaries was observed (Figs. 6a and b). Combination with the SAD and high resolution TEM observations enabled the clear characterization of the structural evolution (Figs. 6c–f). A continuous and amorphous initial (TiVCrZrY)N layer about 6-nm

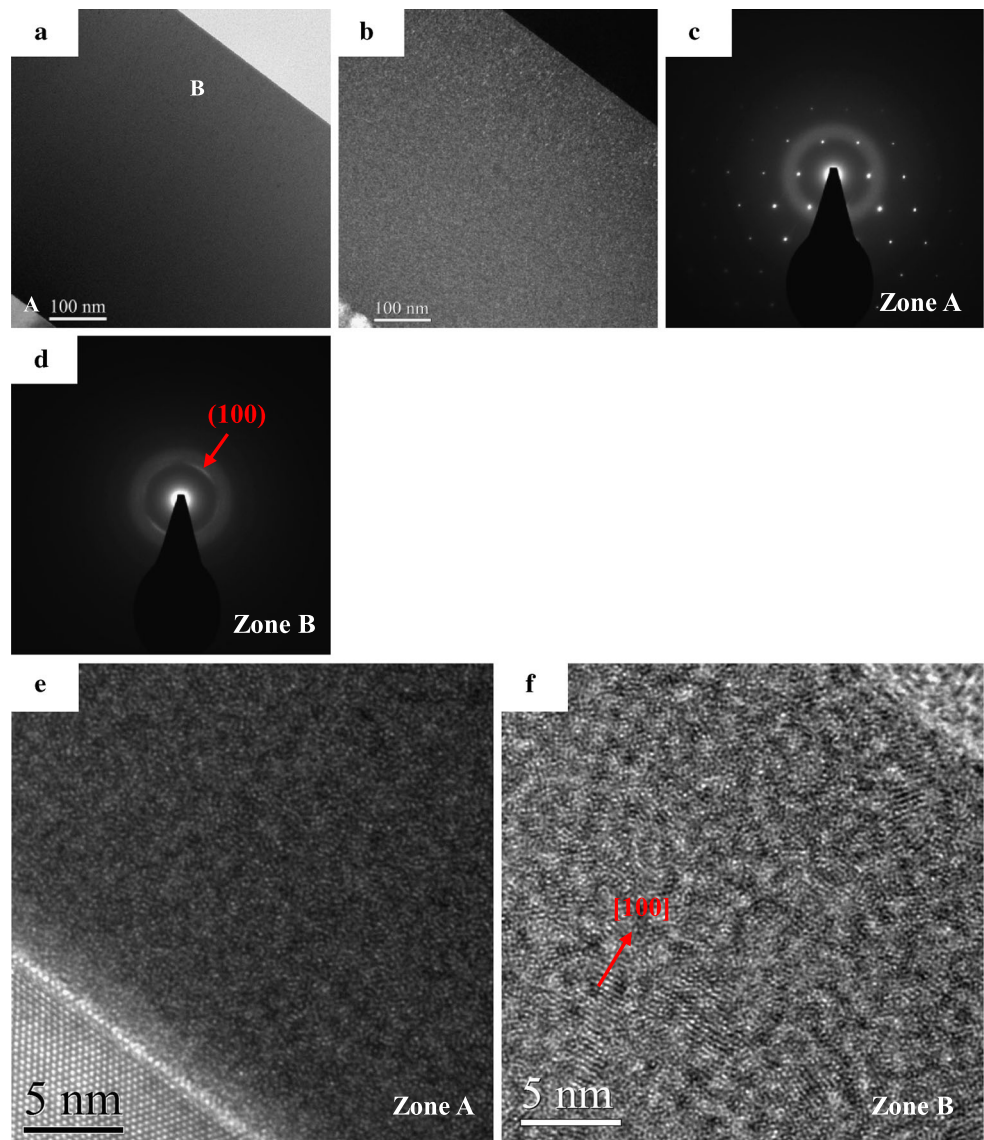
Fig. 4 Plan-view and cross-sectional SEM micrographs of the (TiVCrZrY)N coatings deposited at various R_N : (a) 0 %, (b) 10 %, and (c) 50 %



thick formed on the substrate (Fig. 6e). Afterward, randomly oriented grains nucleated (Fig. 6c) and then grew along the fcc [111] direction of the crystallized grains (Fig. 6d). The top part of the coating structure was confirmed to contain an fcc (200)-axis structure perpendicular to the substrate misaligned at $\sim 54^\circ$ (Fig. 6d). The widths of two columns (zones A and B) were approximately 10–20 and 50 nm, respectively (Figs. 6a and b). These structural changes with the coating thickness were typical for an evolutionary selection growth [27]. In evolutionary selection, the fastest-growing grains with a specific crystallographic orientation enveloped the other grains and determined the final orientation. Hence, the fcc (200) oriented grains were expected to grow fastest at $R_N = 10\%$ in this work and to follow a preferred orientation by enveloping other oriented-grains. Interestingly, the nitride coating had higher crystallinity and larger grain size

than the alloy coating. This finding was reasonable because individual nitrides have the same crystal structure. Therefore, the (TiVCrZrY)N coating tended to form a more crystalline solid solution structure than the alloy coating. As R_N continually increased to 50 %, the original V-shaped columnar feature transformed into a very fine fibrous structure (Figs. 7a and b). The amorphous layer on the substrate thickened to about 80 nm (Fig. 7b). In the SAD pattern (Figs. 7c and d), the results were similar to that of the (TiVCrZrY)N coating deposited at $R_N = 10\%$. However, the rings were broad and weak, indicating poor crystallinity of the coatings near an amorphous structure in accordance with the aforementioned X-ray diffraction analyses. As aforementioned, the relatively large resputtering effect at high R_N was considered to be a dominant reason for the reduced grain size and crystallinity.

Fig. 5 Cross-sectional TEM micrographs of the TiVCrZrY alloy coatings deposited at $R_N = 0\%$. **(a)** Bright-field image. **(b)** Dark-field image using the (110) diffraction rings indicated by circles in the SAD pattern in **(d)**. **(c)** SAD pattern of zone A. **(d)** SAD pattern of zone B. **(e)** High-resolution TEM lattice image of zone A. **(f)** High resolution TEM lattice image of zone B

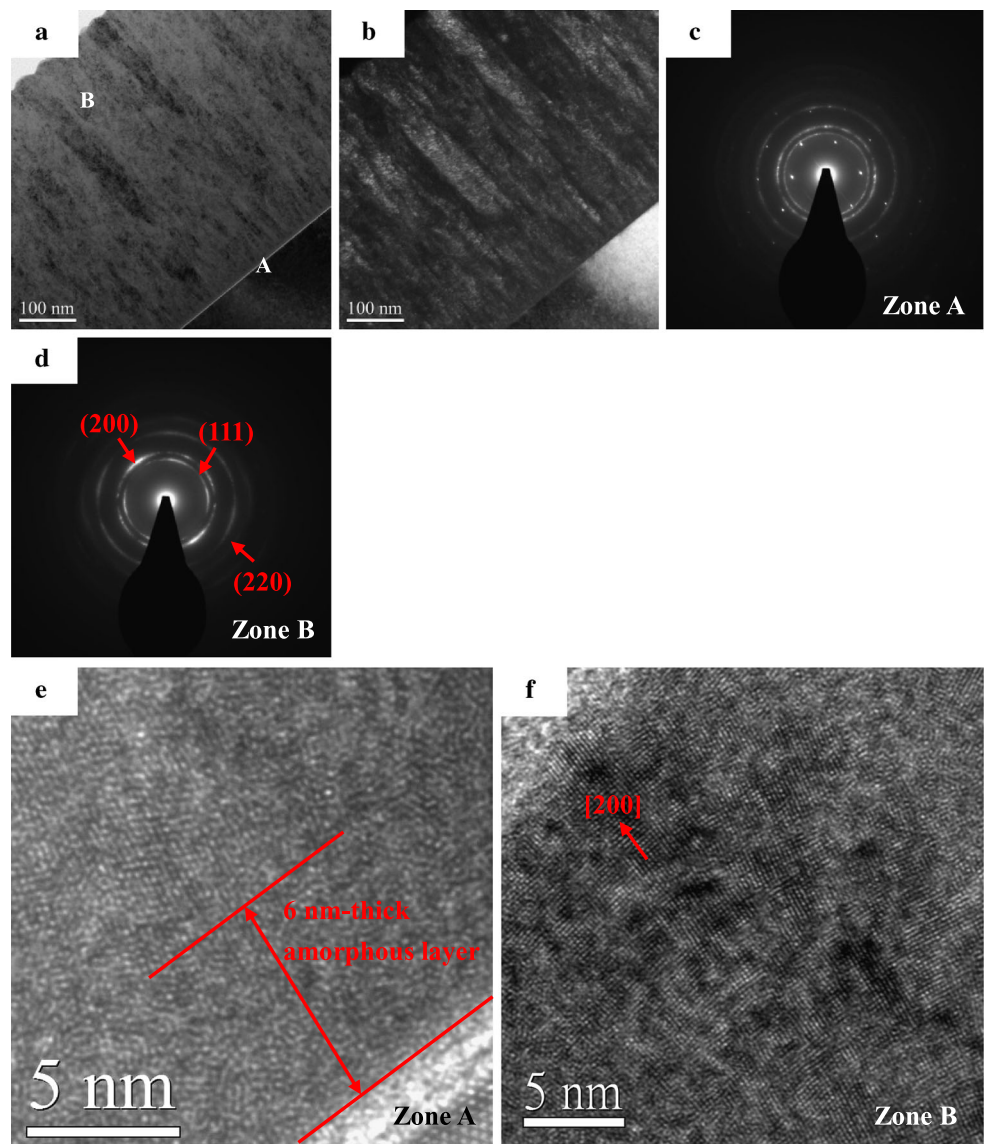


3.3 Properties

Figure 8 shows the hardness and modulus of the (TiVCrZrY)N coatings deposited at various R_N values. For the TiVCrZrY alloy coating deposited at $R_N = 0\%$, the hardness and modulus values were 10.2 and 126 GPa, respectively. These values were higher than those of typical pure metal and alloy coatings and can be attributed to the solid-solution strengthening effect induced by the incorporation of atoms with different sizes. At $R_N = 10\%$, the hardness and modulus greatly increased to 20.9 and 217.4 GPa, respectively. This result can be explained by the formation of a nitride phase and the strong covalent bonding between nitrogen and target elements. As R_N further increased, the hardness and modulus slightly decreased to 18.9 and 188.2 GPa, respectively, possibly because of the grain size. Generally, smaller grain sizes and thus more grain boundaries posi-

tively influence the mechanical properties [28]. Meanwhile, a slip motion may have occurred during deformation. Grain boundaries act as impediments to dislocation motion, and thus the mechanical properties were improved. However, below approximately 10 nm, the grain boundaries tended to slide. If the grain size is too small, fitting the dislocations in the grain is difficult, and the stress required to move them is lower. Consequently, the slight decrease in hardness and modulus results from the slight decrease in grain size [29]. Notably, the (TiVCrZrY)N coatings had significantly low mechanical properties compared with other multielement nitride coatings. The softening may be related to the extremely small grain sizes of 3.5–2.2 nm and poor crystallinity caused by the addition of the large-sized Y atoms. Figure 9 displays electrical resistivity of the (TiVCrZrY)N coatings deposited at various R_N values. The TiVCrZrY alloy coating had a lower electrical resistivity than the nitride coating because

Fig. 6 Cross-sectional TEM micrographs of the TiVCrZrY nitride coatings deposited at $R_N = 10\%$. **(a)** Bright-field image. **(b)** Dark-field image using the (111) and (200) diffraction rings indicated by circles in the SAD pattern in **(d)**. **(c)** SAD pattern of zone A. **(d)** SAD pattern of zone B. **(e)** High-resolution TEM lattice image of zone A. **(f)** High-resolution TEM lattice image of zone B



of the different bond characteristics. As R_N increased, the electrical resistivity significantly increased to a very high value of $21870 \mu\Omega\cdot\text{cm}$ at $R_N = 50\%$. The electrical performance was also possibly dominated by the grain size and crystallinity. This assumption was reasonable because a decrease in the grain size and crystallinity leads to enhanced grain boundary scattering and thus to an increase in electrical resistivity [30, 31].

4 Conclusion

In this study, (TiVCrZrY)N coatings were prepared by the reactive magnetron sputtering of a pure equimolar (TiVCrZrY) target on Si (100) wafers at R_N values ranging from 0% to 50%. The deposited TiVCrZrY alloy and nitride coatings possessed an hcp and fcc solid-solution struc-

ture, respectively. The TiVCrZrY alloy coating deposited at $R_N = 0\%$ exhibited a very dense and smooth equiaxed structure. With the introduction of nitrogen, crystalline nitride structure formed. The (TiVCrZrY)N coating deposited at $R_N = 10\%$ revealed a V-shaped columnar structure with rough surfaces, which was typical for an evolutionary overgrowth mechanism. The microstructure was still dense but contained relatively better crystallinity and larger grain sizes. A 6-nm-thick amorphous phase was also observed near the substrate. The hardness and electrical resistivity were measured to be around 20.9 GPa and $398.2 \mu\Omega\cdot\text{cm}$, respectively. As the R_N was increased from 10% to 50%, the microstructure of the nitride coatings was converted to a fine fibrous structure. The amorphous layer gradually thickened to 80 nm, and the crystallinity and grain size gradually deteriorated. These phenomena were attributed to the enhanced resputtering effect at higher R_N . The hardness

Fig. 7 Cross-sectional TEM micrographs of the TiVCrZrY nitride coatings deposited at $R_N = 50\%$. (a) Bright-field image. (b) Dark-field image using the (111) and (200) diffraction rings indicated by circles in the SAD pattern in (d). (c) SAD pattern of zone A. (d) SAD pattern of zone B. (e) High-resolution TEM lattice image of zone A. (f) High-resolution TEM lattice image of zone B

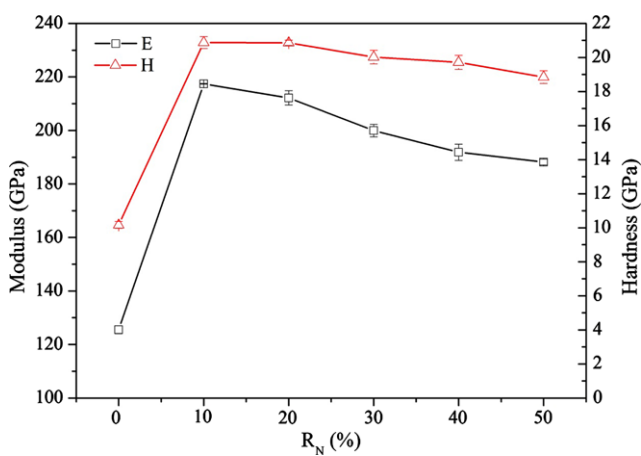
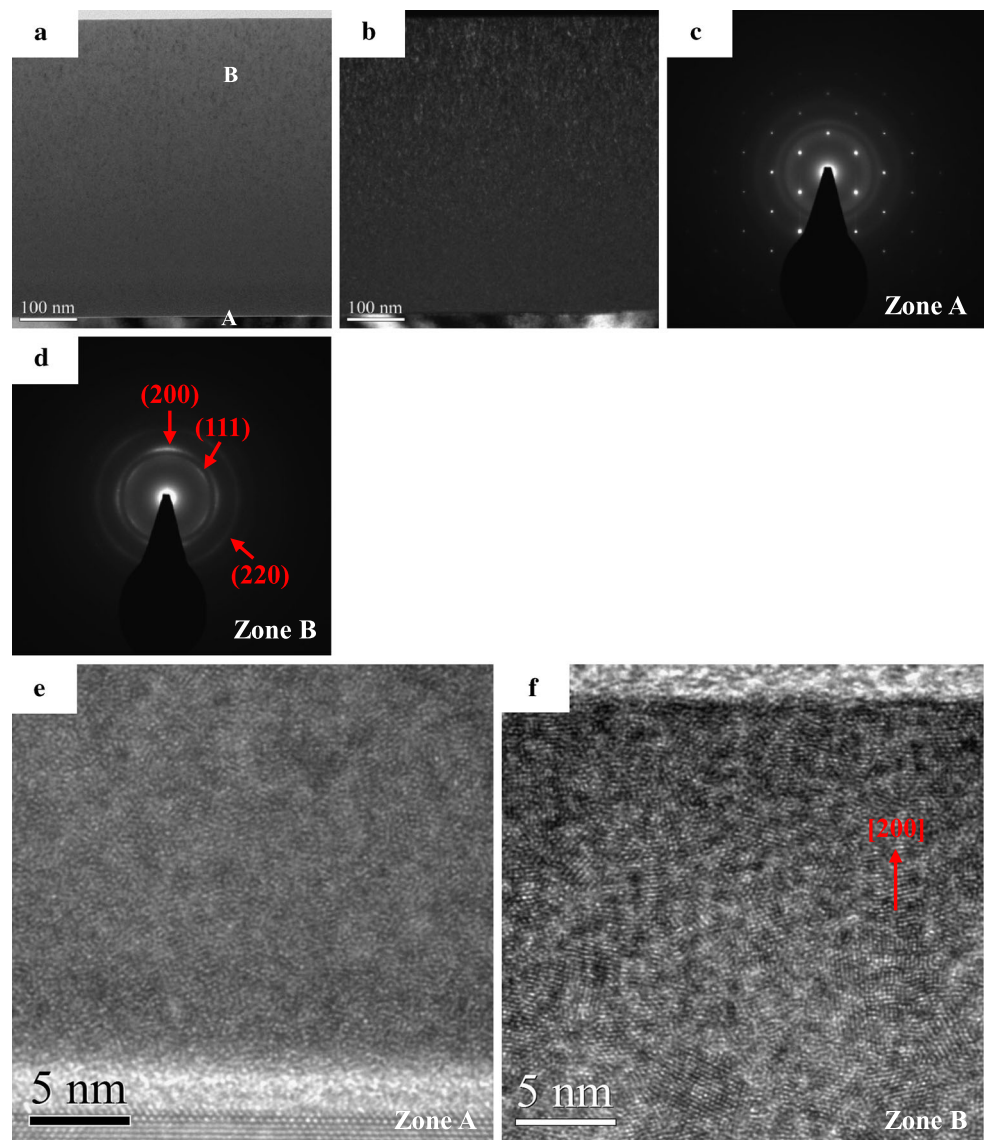


Fig. 8 Hardness and modulus of the (TiVCrZrY)N coatings deposited at various R_N

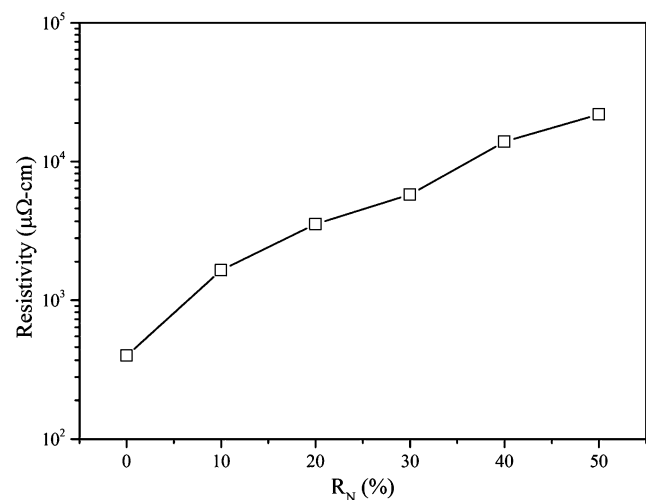


Fig. 9 Electrical resistivity of the (TiVCrZrY)N coatings deposited at various R_N

and electrical resistivity deteriorated to nearly 18.9 GPa and 21870 $\mu\Omega\cdot\text{cm}$, respectively, which can be attributed to the grain size and crystallinity. Compared with other published multielement nitride coatings, the (TiVCrZrY)N coatings exhibited a very small grain size and poor crystallinity mainly because of the relatively large atomic size difference.

References

- H.O. Pierson, *Handbook of Refractory Carbides and Nitrides*, (Noyes, New Jersey, 1996)
- V. Chawla, R. Jayaganthan, R. Chandra, *Mater. Charact.* **59**, 1015–1020 (2008)
- M. Popović, M. Novaković, N. Bibić, *Mater. Charact.* **60**, 1463–1470 (2009)
- Y. Wang, X. Yan, B. Li, G. Tu, *Int. J. Refract. Met. Hard Mater.* **30**, 200–207 (2012)
- L. Zhu, M. Hu, W. Ni, Y. Liu, *Vacuum* **86**, 1795–1799 (2012)
- D.M. Devia, E.R. Parra, P.J. Arango, A.P. Tschiptschin, J.M. Velez, *Appl. Surf. Sci.* **257**, 6181–6185 (2011)
- C.H. Hsu, C.K. Lin, K.H. Huang, K.L. Ou, *Surf. Coat. Technol.* (2012). doi:10.1016/j.surfcoat.2012.05.095
- Z.Z. Tang, *Ceram. Int.* **38**, 2997–3000 (2012)
- H. Hasegawa, A. Kimura, T. Suzuki, *J. Vac. Sci. Technol. A* **18**, 1038–1040 (2000)
- B. Ren, Z. Shen, Z. Liu, *J. Alloys Compd.* **560**, 171–176 (2013)
- P.K. Huang, J.W. Yeh, *Surf. Coat. Technol.* **203**, 1891–1896 (2009)
- K.H. Cheng, C.H. Lai, S.J. Lin, J.W. Yeh, *Thin Solid Films* **519**, 3185–3190 (2011)
- M.H. Tsai, C.H. Lai, J.W. Yeh, J.Y. Gan, *J. Phys. D* **41**, 235402 (2008)
- S.C. Liang, D.C. Tsai, Z.C. Chang, H.S. Sung, Y.C. Lin, Y.J. Yeh, M.J. Deng, F.S. Shieu, *Appl. Surf. Sci.* **258**, 399–403 (2011)
- M. Uchida, N. Nihira, A. Mitsuo, K. Toyoda, K. Kubota, T. Aizawa, *Surf. Coat. Technol.*, **177–178**, 627–630 (2004)
- D.C. Tsai, Y.L. Huang, S.R. Lin, S.C. Liang, F.S. Shieu, *Appl. Surf. Sci.* **257**, 1361–1367 (2010)
- H.P. Klug, L.E. Alexander, *X-Ray Diffraction Procedures for Polycrystalline and Amorphous Materials* (Wiley, New York, 1974)
- R.M. Mason, M. Pichiling, *J. Appl. Phys.* **32**, 365–369 (1961)
- D.C. Tsai, F.S. Shieu, S.Y. Chang, H.C. Yao, M.J. Deng, *J. Electrochem. Soc.* **157**, K52–K58 (2010)
- D.C. Tsai, Y.L. Huang, S.R. Lin, D.R. Jung, S.Y. Chang, F.S. Shieu, *J. Alloys Compd.* **509**, 3141–3147 (2011)
- J. Musil, H. Poláková, *Surf. Coat. Technol.* **127**, 99–106 (2000)
- J. Pelleg, L.Z. Zevin, S. Lungo, N. Croitoru, *Thin Solid Films* **197**, 117–128 (1991)
- F. Shinoki, A. Itoh, *J. Appl. Phys.* **46**, 3381–3384 (1975)
- D.C. Tsai, S.C. Liang, Z.C. Chang, T.N. Lin, M.H. Shiao, F.S. Shieu, *Surf. Coat. Technol.* **207**, 293–299 (2012)
- Y. Zhang, Y.J. Zhou, J.P. Lin, G.L. Chen, P.K. Liaw, *Adv. Eng. Mater.* **10**, 534–538 (2008)
- V. Braic, A. Vladescu, M. Balaceanu, C.R. Luculescu, M. Braic, *Surf. Coat. Technol.* **211**, 117–121 (2012)
- A. van der Drift, *Philips Res. Rep.* **22**, 267–288 (1967)
- S. Veprek, *J. Vac. Sci. A* **17**, 2401–2420 (1999)
- R.W. Siegel, G.E. Fougere, *Nanostruct. Mater.* **6**, 205–216 (1995)
- J.D. Plummer, M.D. Deal, P.B. Griffin, *Silicon VLSI Technology: Fundamentals Practice and Modeling* (Prentice-Hall, Englewood Cliffs, 2000)
- W.D. Sproul, J.E. Greene, J.A. Thornton, *Physics and Chemistry of Protective Coatings* (American Institute of Physics, New York, 1986)